Characterization of SiO_2 Nanoparticles by Single Particle – Inductively Coupled Plasma – Tandem Mass Spectrometry (SP-ICP-MS/MS)

Eduardo Bolea-Fernandez[a], Diego Leite[b], Ana Rua-Ibarz[a], Lieve Balcaen[a], Maite Aramendía[bc*], Martín Resano[b], Frank Vanhaecke[a]

[a]Ghent University, Department of Analytical Chemistry, Campus Sterre, Krijgslaan 281-S12, 9000 Ghent, Belgium

[b]University of Zaragoza, Aragón Institute of Engineering Research (I3A), Department of Analytical Chemistry, Pedro Cerbuna 12, 50009 Zaragoza, Spain

[c]Centro Universitario de la Defensa, Carretera de Huesca s/n, 50090 Zaragoza, Spain

[*]Corresponding author

ABSTRACT

The increase in the use of SiO_2 nanoparticles (NPs) is raising concern about their environmental and health effects, thus necessitating the development of novel methods allowing for their straightforward detection and characterization. Single Particle ICP- mass spectrometry (SP-ICP-MS) is able to provide information on the size of NPs, their particle number density and mass concentration. However, the determination of Si *via* ICP-MS is strongly hampered by the occurrence of spectral overlap from polyatomic species (e.g., CO^+ and N_2^+).

The use of tandem ICP-MS (ICP-MS/MS) enables interference-free conditions to be obtained, even in the most demanding applications. Upon testing of several gases, the use of CH_3F (monitoring of SiF^+, mass-shift approach) and of H_2 (monitoring of Si^+, on-mass approach) were demonstrated to be the most suitable to overcome the spectral interference affecting ultra-trace Si determination (LoD < 15 ng L^{-1}). By using these approaches, SiO_2 NPs (ranging between 80 and 400 nm) can be detected and characterized. For SiO_2 NPs > 100 nm, it was possible to provide accurate results in a straightforward way, as the signals they give rise to are well resolved from that of the background. In the case of 80 and 100 nm NPs, the use of a simple deconvolution approach following a Gaussian model was needed to characterize SiO_2 NPs apparently showing incomplete distributions as a result of the presence of the background signal. Overall, the methods developed using SP-ICP-MS/MS are sensitive and selective enough for interference-free determination of Si at ultra-trace levels, also under the form of SiO_2 NPs.

1. INTRODUCTION

Due to their unique physical and chemical properties, the use of nanomaterials is rapidly growing over the last years.[1] As non-metal oxides, SiO_2 nanoparticles (NPs) are used in a large variety of applications, such as in food additives, drugs, coatings, sensors and cosmetics.[2-4] Furthermore, SiO_2 NPs are widely employed for chemical mechanical planarization (CMP), in which their abrasive properties are relied on to polish materials in the semiconductor industry.[5] This massive use of NPs is raising concern about their potential effects on the environment and human health,[6-8] and different international directives exist (*e.g.,* from the European Commission), urging the need to characterize such materials.[9] However, the development of analytical methods that are able to gather information on the main physicochemical properties, such as particle number density and mass concentration, degree of particle aggregation and size distribution of NPs present in different sample matrices, remains a challenging task.[10] Despite the considerable amount of techniques currently available for characterizing nanomaterials, *e.g.*, differential centrifugal sedimentation (DCS), nanoparticle tracking analysis (NTA), dynamic light scattering (DLS), static light scattering (SLS), scanning electron microscopy (SEM) and transmission electronic microscopy (TEM),[4, 10, 11] significant limitations, such as cost, time of analysis, lack of elemental specificity, incompatibility with some sample matrices and relatively high limits of detection (mg L^{-1}), still exist.[12, 13]

Single particle – inductively coupled plasma – mass spectrometry (SP-ICP-MS) is a powerful and emerging technique for routine analysis of NPs, which provides a wide range of information, typically elemental composition, particle size, particle number density, mass concentration, and size distribution.[14-17] SP-ICP-MS enables for characterization of NPs in samples with complex matrices, such as those encountered in environmental and clinical applications.[18] In SP mode, ICP-MS is operated in time-resolved analysis (TRA) mode, in which it is capable to detect, count and register NP signals as their corresponding set of pulses collected over a number of subsequent short dwell times. Particle size and particle number density can be calculated based on the intensity of these pulses and

their frequency, respectively, while both are used to provide mass concentration.[19] Although this technique has been developed and refined in recent years, many aspects are still susceptible to improvement, especially for applications for which pronounced spectral overlap jeopardizes accurate ICP-MS analysis.[17, 20, 21] This is the case for SiO_2 NPs, the determination of which is hampered by the occurrence of spectral interferences coming from elements ubiquitously present in the plasma itself, (e.g., giving rise to signals from $^{14}N^{14}N^{+}$ and $^{12}C^{16}O^{+}$, overlapping with the signal of the most abundant Si isotope at m/z = 28). Thus, the development of novel strategies to tackle the problem of spectral overlap in ICP-MS is required when aiming at obtaining reliable SiO_2 NPs characterization *via* SP-ICP-MS.

The use of high resolution sector-field ICP-MS (HR-SF-ICP-MS) instrumentation is an elegant approach to deal with spectral interferences.[22] With this technique, analyte and interfering ions can be separated from each other by increasing the resolution of the double-focusing sector-field mass analyzer. However, an increase in mass resolution is typically accompanied by a significant reduction in ion transmission efficiency, and thus, in sensitivity (1 – 2 orders of magnitude).[23, 24] In addition, the more recent developments in the field of SP-ICP-MS have been made in quadrupole-based ICP-MS (ICP-QMS) instruments, especially those related with detection speed and data treatment,[25] which probably explains why SP-ICP-MS has been mainly conducted with ICP-QMS instruments so far. However, the low mass resolution attainable with a quadrupole mass analyzer (1 amu) is to be considered a major limitation in the applicability of SP-ICP-MS for elements affected by spectral interference, especially for complex sample matrices.

The relatively recent (2012) introduction of ICP-tandem mass spectrometry (ICP-MS/MS) was a significant breakthrough as the MS/MS approach substantially enhances the capabilities of ICP-QMS for avoiding spectral interference.[26, 27] ICP-MS/MS instruments are equipped with two quadrupole units (Q1 and Q2), and a collision/reaction cell (CRC) located in-between these two quadrupoles, thus enabling for a double mass selection. In the MS/MS mode, all ions with a mass-to-charge ratio (m/z)

different from that of the target nuclide are filtered out by Q1, thus enhancing the control over the collisions/reactions taking place in the CRC and permitting a much more efficient resolution of interferences.[28, 29]

Over the last years, selective ion-molecule chemistry in the CRC in ICP-MS/MS instrumentation (usually referred to as chemical resolution) has been relied on for the interference-free determination of ultra-trace concentrations of several analytes in the most diverse and complex sample matrices. In addition to the more common collision/reaction gases (e.g., He, H_2 and/or O_2), the potential of using highly reactive gases, such as NH_3 or CH_3F, has been demonstrated.[30-32] However, the determination of ultra-trace concentrations of Si *via* ICP-MS/MS has been hindered by strong spectral overlap affecting all of the Si isotopes, and only a few works to date have reported on such determinations.[33, 34] In addition, chemical resolution as a means to avoid spectral interference in ICP-MS/MS has been scarcely used in the context of NPs characterization. The applications reporting on the use of chemical resolution for NPs studies mostly involved the use of field-flow fractionation (FFF).[35-37]

This work assesses the potential of ICP-MS/MS for creating interference-free conditions for ultra-trace Si determination, aiming at the characterization of SiO_2 NPs *via* SP-ICP-MS/MS.

2. EXPERIMENTAL

2.1. Standards, samples and reagents.

Ultra-pure water (resistivity > 18.2 MΩ cm) was obtained from a Mili-Q Element water purification system (Millipore, France). Appropriate dilutions from a 1 g L^{-1} single-elemental standard solution of Si (Instrument Solutions, The Netherlands) were prepared freshly on a daily basis and were used for method development and calibration purposes (concentrations ranging between 0 and 5 µg L^{-1} under the form of dissolved Si). SiO_2 NPs suspended in water were obtained from nanoComposix (non-functionalized NanoXact™ Silica, Czech Republic). Particle size distributions, particle number density and mass concentration for these suspensions (determined by TEM and gravimetric analysis, respectively) were provided by the manufacturer. Table 1 provides a compilation of all relevant information for the stock solutions. For the purpose of counting and sizing SiO_2 NPs, a reference material NIST SRM 8013 – Gold Nanoparticles (AuNPs), of 60 nm nominal diameter (certified diameter: 56.0 ± 0.5 nm) – was used for determining transport efficiency in the ICP-MS instrument used. All NP suspensions were shaken vigorously and sonicated during 10 minutes before their use to avoid particle agglomeration. To minimize the occurrence of double events in SP-ICP-MS mode, appropriate dilutions of the original NP suspensions were prepared. To calculate the dilution factor needed for each of the NP suspensions analyzed, probability calculations based on Poisson statistics were carried out taking into account the exact experimental parameters finally selected for the measurements (*i.e.* dwell time, transport efficiency and sample uptake rate) as to ensure a probability of double events to occur below 5 %.[38] For the suspensions of NPs with a diameter below 100 nm, for which the particle distribution signal partially overlapped with that of the background, lower dilution factors leading to increased probabilities of double events were used, as discussed in section 3.2.2. Final dilution factors used for all of the NP suspensions measured are also included in Table 1.

2.2. Instrumentation

All measurements were carried out using an Agilent 8800 "triple quadrupole" ICP-MS/MS instrument (Agilent Technologies, Japan). The sample introduction system comprises a Micromist nebulizer (400 µL min^{-1}) and a Peltier-cooled Scott-type spray chamber (2 °C). The instrument is equipped with two quadrupole mass analyzers (Q1 and Q2) and an octopole collision-reaction cell (ORS^3) mounted in-between the two quadrupole units (Q1-ORS-Q2). The tandem mass spectrometry configuration enables this instrument to be operated in two different modes, single quadrupole (SQ) and MS/MS mode. In SQ mode, Q1 is fully open, while in MS/MS mode, both quadrupoles are used as mass filters with a single-mass bandpass window. Therefore, the MS/MS mode provides an improved control over the collisions/reactions occurring within the ORS. This setup also offers precursor and/or product ion scanning as powerful tools for method development, especially in the context of interference removal. In this work, the ORS was pressurized with various inert (He) and reactive (H_2, O_2, NH_3/He (10% NH_3 in He) and CH_3F/He (10% CH_3F in He)) gases; also the no gas or "vented" mode was evaluated for illustrative purposes (the most relevant ICP-MS/MS instrument settings used are listed in Table 2). All gases were introduced in the instrument *via* their corresponding inlets, except for the mixture of CH_3F/He that was introduced *via* the 4th line, which is originally intended for the use of O_2. Therefore, the CH_3F/He gas flow rates will be reported as their equivalent O_2 gas flow rates owing to the calibration of the gas flow controller for the latter. Although NH_3 and CH_3F were used as their corresponding mixtures with 90% He, they will be further referred in this text to as NH_3 and/or CH_3F reaction gases.

2.3. Data treatment

The raw data obtained using the Agilent ICP-MS MassHunter Software operated in Time Resolved Analysis (TRA) mode were treated and evaluated externally using a modified spreadsheet previously described by Peters *et al.*[39] This spreadsheet is composed of two interrelated worksheets used for calibration and NPs characterization, respectively. For calibration, the transport efficiency (*i.e.* nebulization efficiency) was determined using NIST SRM 8013 AuNPs. This characteristic was

determined according to the method described by Pace *et al.,*[40] which takes into account known mass concentration and particle size and the corresponding pulse frequency observed for calculating the transport efficiency. In the second worksheet, particle number density, mass concentration and particle size distribution are calculated for each sample by means of the response factor determined using the ionic Si standard solutions and the transport efficiency. To decide whether NP pulses differ significantly from the background signal, the 3s-criterion (3 times the standard deviation of the background) is relied on.

For SiO_2 NP distributions that are difficult to discern from the background, a simple deconvolution approach using OriginLab was used for modeling. This approach relies on approximating the raw distribution by a Gaussian model. The equation thus obtained was used to calculate the particle diameter, particle number density and mass concentration (see section 3.2.2.).

3. RESULTS AND DISCUSSION

3.1. Method development for interference-free determination of Si *via* ICP-MS/MS

As discussed in the introduction, interference-free determination of ultra-trace concentrations of Si *via* ICP-QMS remains as a challenging task. The occurrence of strong spectral overlap of the signal of the major isotope of Si (^{28}Si – 92.23 % relative isotopic abundance) and polyatomic species (e.g., CO^+ and N_2^+) can jeopardize the ability to distinguish the background signal from the signals generated by SiO_2 NPs. Therefore, the development of novel methods to overcome spectral interferences is a prerequisite for enabling determination of very low Si concentrations and/or to characterize SiO_2 NPs. ICP-MS/MS has demonstrated to be a powerful tool to investigate the reactions occurring within the collision/reaction cell (CRC) and to develop novel approaches to eliminate or at least mitigate spectral overlap.[28, 29] In MS/MS mode, *i.e.* in which both quadrupoles are set at a specific m/z ratio, the cell was operated under different conditions: (*i*) no gas or "vented mode", (*ii*) He "kinetic energy discrimination (KED) mode" and (*iii*) H_2, O_2, NH_3 and/or CH_3F "chemical resolution modes". In contrast to "vented" or "KED" modes, in which Q1 and Q2 are set at m/z 28, the use of chemical

resolution, where the interferences are overcome by selective ion-molecule chemistry, the selection of the Q2 setting is not always self-evident. *Via* product ion scanning (PIS), with Q1 fixed at m/z = 28 and the cell pressurized with different reaction gases at different flow rates, the reactivity of Si towards these gases was evaluated by means of scanning the entire mass spectrum (2 – 260 amu) with Q2. Figure 1 shows an example of the mass spectra obtained in the region 2 – 100 amu (where most of the product ions appear) for the different chemical resolution modes, and using the optimum gas flow rate for maximizing the sensitivity for the reaction product ions that were finally selected. Analysis of the full set of PIS spectra obtained at different gas flow rates allowed for the selection of the best-suited reaction product ions. In particular, SiH^+ (+1, m/z=29), SiO^+ (+16, m/z=44), $SiNH_2^+$ (+16, m/z=44) and SiF^+ (+19, m/z=47) were the reaction product ions selected for Si determination. In addition to mass-shift approaches, the use of H_2 in an on-mass approach was evaluated for its capability to remove CO^+ and N_2^+ polyatomic interferences *via* reaction towards H_2. For fine-tuning, the optimum gas flow rates for every method were selected such as to maximize the signal-to-background ratio (intensity for 5 µg L^{-1} Si in MQ H_2O) using the "ramp cell gas" option available in the instrument's software. Results for this optimization are shown in Figure 2. In this figure, the initial improvement in ion sensitivity observed at low flow rates for the H_2 – on mass approach might seem surprising. However, this fact can most likely be attributed to a collisional focusing effect typical for instruments equipped with collision/reaction cells.[41, 42] Despite the fact that interference-free conditions were achieved, the remnant background signals obtained for every m/z monitored and every reaction gas investigated correspond in all cases to a BEC of 0.29 ± 0.02 µgL^{-1} Si, which seems to indicate that there was a slight dissolved Si contamination in the MQ water used, an issue well documented for Si determination.[43, 44] Table 3 summarizes the different reaction pathways of analyte and interfering ions for the different operation modes evaluated in this work.

Furthermore, in addition to the MS/MS mode, the different approaches developed were tested for their capabilities to avoid spectral overlap when the instrument was operated in single quadrupole (SQ) mode *i.e.*, Q1 fully open. SQ was evaluated as a possible approach in the case of "vented" mode

and of H_2 – on-mass, while for O_2, NH_3 and CH_3F, the background signal was found to be very high due to the occurrence of spectral interferences at the m/z ratios of the reaction product ions selected. This may be related with the formation of unwanted product ions in the CRC, especially for highly reactive gases, such as NH_3 and CH_3F. For H_2 – mass-shift, however, the signal of $^{28}SiH^+$ overlapped with that of other Si isotope (^{29}Si – 4.69 % abundance), thus only allowing to preserve the Si isotopic pattern by using MS/MS mode. For 5 µg L^{-1} Si, the signal-to-background ratio for He (KED mode) was found to be compromised by a strong reduction in sensitivity; this reduction was even more pronounced in SQ, and therefore, this approach was not further considered in the context of this work.

Once the different methods were optimized, calibration data and instrumental limits of detection (LoDs) and of quantification (LoQs) were calculated by measuring 5 standard solutions (concentration ranging between 0 and 5 µg L^{-1} Si). The results obtained for the different operation modes are summarized in Table 4. Instrumental LoDs and LoQs were calculated as 3 and 10 times the standard deviation on 10 consecutive measurements of a blank solution (MQ H_20), divided by the slope of the calibration curve, respectively. Even in vented mode, a reduction of the background signal and an improvement in the signal-to-background ratio was seen when switching from SQ to MS/MS mode, which can be attributed to a better transmission efficiency for atomic ions (Si^+) throughout the tandem mass spectrometer than for polyatomic ions (*e.g.*, CO^+ and N_2^+). Selection of the best approaches was based on the sensitivity of the corresponding method and on the ability to create interference-free conditions (best BEC approach[45]). Hence, the use of He (KED mode) and of O_2 (mass-shift – SiO^+) were considered less suitable owing to the poor sensitivity in the first case, and the possible occurrence of spectral interferences in the second (see Table 3), which could become relevant in cases where the sample matrix contains higher concentrations of C and/or N (e.g., added nitric acid or organic solvents). In the case of O_2, it was also evaluated whether increasing the O_2 gas flow rate for monitoring SiO_2^+ as reaction product ion would result in a method suitable for Si determination. However, although this approach was successfully applied by Gourgiotis *et al*.[46] in the

context of isotopic analysis of Si for alteration studies of nuclear waste glasses, the method obtained was not sufficiently sensitive for ultra-trace Si determination.

As a conclusion, the use of H_2 (on-mass and mass-shift) and of NH_3 and CH_3F (mass-shift) seem to be the methods of choice for the determination of Si at low concentration levels. As indicated in Table 4, instrumental LoDs ranging between 0.01 and 0.05 µg L^{-1} were achieved using these approaches (*i.e.* chemical resolution in MS/MS mode). With H_2 (on-mass), the highest sensitivity was obtained, but with CH_3F (mass-shift), the lowest LoD was provided. Thus, these two methods were selected for further SP-ICP-MS/MS method development, although results of other approaches will be provided for comparative purposes.

3.2. Analysis of SiO_2 NPs *via* SP-ICP-MS/MS

3.2.1. Detection of SiO_2 NPs

Once the different approaches were optimized for interference-free determination of ultra-trace concentrations of Si, their suitability for characterizing SiO_2 NPs was evaluated. As described in the experimental section, NIST SRM 8013 (AuNPs) was used to determine the transport efficiency, which is required in order to convert the particle detection rate obtained for SiO_2 NPs into the particle number density. The transport efficiency was found to be 7.2 ± 0.4 %, without significant variations between experimental sessions.

For SP-ICP-MS/MS, the measurement of fast transient signals with a dwell time < 10 ms in Time Resolved Analysis (TRA) mode should enable the detection of every single NP. In this context, the dwell time is an important parameter that needs to be carefully selected considering the characteristics of the ICP-MS instrument used. In this respect, there are two main types of ICP-MS instruments: those allowing for dwell times in the µs range and those only allowing for dwell times in the ms range, each requiring a different approach for selecting the optimum dwell time. When the minimum dwell time allowed by the ICP-MS instrument deployed is significantly shorter than the typical duration of an ICP-MS intensity spike caused by a single particle (about 0.5 ms according to literature),[38, 47] dwell times in the range of 100 µs are preferred to minimize the background

contribution to the signal of each NP. However, when the minimum dwell time allowed by the ICP-MS instrument deployed is longer than the typical signal due to a single particle, the best option seems to select a dwell time sufficiently low to minimize the background contribution to the signal, but long enough to minimize the probability of splitting the signal of a single NP in various events.[38] Additionally, the particle number density of the NP dispersions measured is also critical in this methodology as the probability of measuring two or more NPs in a single dwell time needs to be minimized. In this regard, there tends to be an agreement in the SP-ICP-MS community to use dwell times of 3-5 ms as the most suitable for instruments allowing dwell times in the ms range only.[14, 39] In the particular case of SiO_2 NPs, and due to the occurrence of contamination issues affecting ultra-trace Si determination, a dwell time of 3 ms (the shortest time selectable for the Agilent 8800 ICP-MS/MS instrument) was finally chosen. Once this selection was made, and as described in detail in section 2.1, all NP suspensions to be measured with the optimized parameters were adequately diluted with MQ water to minimize the occurrence of double events. Final dilution factors used for all of the NP suspensions measured are included in Table 1.

At this point, it is fair to indicate that the use of dwell times in the order of 100 µs has been reported on in literature as an additional means to improve the detection capabilities of SP-ICP-MS for smaller NPs,[20, 25, 48] including SiO_2.[49] As previously indicated, the use of this approach requires instrumentation allowing for ultrafast acquisition of data (every 100 µs), as well as additional data treatment to identify the different events detected for every NP, and an evaluation of this possibility was beyond the scope of this work.

As a next step, the different methods developed in the previous section were tested for their capability to distinguish the signals from a given SiO_2 NP suspension from the background signal. First, the theoretical size limits of detection (LoD_{size}) for every approach were calculated as described by Laborda *et al.*[14] (see Equation 1).

$$LOD_{size} = \left(\frac{18 s_B}{\pi \rho X_{NP} K_{ICPMS} K_M}\right)^{1/3} \quad \text{Equation 1}$$

where s_B is the standard deviation of the continuous background measured in SP-ICP-MS/MS mode, ρ the density of the NPs, X_{NP} the mass fraction of the element monitored in the NP, K_{ICPMS} the detection efficiency (ratio of the number of ions detected *vs* the number of atoms introduced into the ICP) and K_M ($=AN_{AV}/M_M$) where A is the atomic abundance of the isotope measured, N_{AV} the Avogadro number, and M_M the atomic mass of the analyte M. For S_B calculation in each measurement mode, all of the SiO_2 NP suspensions and the water blank provided similar results, indicating that the potential effect of the introduction of larger NPs on the plasma conditions (e.g., plasma cooling)[2, 38] was negligible for the range of NP sizes evaluated. Theoretical $LoDs_{size}$ determined according to Equation 1 were 50 nm (H_2), 70 nm (CH_3F), 80 nm (O_2), 80 nm (NH_3), 90 nm (no gas) and 160 nm (He).

Figure 3 shows the practical $LoDs_{size}$ using the different approaches evaluated in this work obtained from the frequency distributions for the dispersions of the smallest of the NPs tested that could be actually differentiated from the background. As seen from this figure, these practical $LoDs_{size}$ corresponded with 75 nm (H_2 – on-mass), 85 nm (CH_3F – mass-shift), 125 nm (no gas or "vented" mode and NH_3 – mass shift), 130 nm (O_2) and 290 nm (He – on-mass). From these results, it is evident that practical $LODs_{size}$ are always higher than theoretical $LODs_{size}$; this is especially noticeable for the He – on-mass mode. These differences could be related with the relatively high BEC observed in all measurements due to slight dissolved Si contamination, as indicated before. Thus, the use of higher purity water and/or of controlled environments (such as clean room facilities) may allow smaller NPs to be detected using the same approaches. At this point, it is also interesting to point out that, in the case of no gas or "vented" mode, the LoD_{size} will increase with the addition of elements at the origin of polyatomic interferences (*i.e.* N and/or C). In any case, it seems clear that the use of H_2 (Si^+, on-mass) and of CH_3F (SiF^+, mass-shift) appear to be the best approaches for SiO_2 NP characterization. Figure 4 shows the frequency distribution (*i.e.* number of particles detected) of SiO_2 NPs with diameters ranging from 80 to 400 nm as a function of signal intensity (cps) when using H_2 – on-mass. It can be seen that, while the signals for NPs with diameters of 80 and 100 nm are partially obscured

by the background signal, the signals of NPs > 100 nm are found to be completely resolved by using this approach, thus enabling for the determination of their particle size, particle number density and mass concentration.

3.2.2. Characterization of SiO_2 NPs

As indicated before, H_2 – on-mass and CH_3F – mass-shift were the methods selected in this work for characterizing SiO_2 NPs. Once detected, the ICP-MS intensity spike generated by a single NP enables its size (NP diameter) to be determined, while the number of events recorded during the analysis time (frequency) allows for the concentration (number of particles per volume unit) to be characterized. As previously indicated, all measurements were performed using a dwell time of 3 ms and monitoring the transient signals during 60 s. Three measurement replicates were done for every SiO_2 NP suspension. As explained in detail in section 2.1, the concentrations of these suspensions were optimized in the range of 0.1 to 5 µg L^{-1} of Si in order to reduce the probability of double events and/or to avoid detector saturation from occurring without compromising counting statistics for NP distributions. The final dilution factors used for each measurement are included in Table 1. Raw data were treated using a modified spreadsheet previously described by Peters *et al.,*[39] as indicated in section 2.3. The SiO_2 particle number density in each suspension (particles L^{-1}) was calculated taking into account the number of NP events detected, the transport efficiency and the sample flow rate (previously calculated and corresponding to 0.34 mL min^{-1}). The mass concentration in each NP suspension was determined based on (*i*) the net intensity measured for a single NP event (after background subtraction), (*ii*) the corresponding sensitivity for Si under the different conditions evaluated (which was calculated during every measurement session), (*iii*) the sample flow rate, (*iv*) the transport efficiency and (*v*) the molar mass ratio SiO_2/Si (2.14). Thereafter, the NP diameter was calculated as a function of the NP mass and its density, assuming that SiO_2 NPs are spherical.

This approach was used to calculate particle size, particle number density and mass concentration of SiO_2 NP suspensions ranging from 80 to 400 nm using H_2 (on-mass) and CH_3F (mass-shift). Figure 5 shows the distributions obtained for different SiO_2 NP sizes as normalized frequency (number of NPs

of each diameter detected divided by the number of NPs detected with the diameter at the peak maximum) *vs* diameter (nm). As already indicated in section 3.2.1 (see Figures 3 and 4), the distributions for NPs with diameters higher than 100 nm were found to be completely resolved from that of the background signals, therefore allowing for a straightforward characterization of these SiO_2 NPs. However, for NPs of 100 nm (CH_3F – mass-shift approach) and of 80 and 100 nm (H_2 – on-mass approach), Figure 5 shows a partial overlap of the NP distribution with that of the background signals. The results of particle diameter (nm), particle number density and mass concentration (recoveries, %) obtained with this approach are provided in Table 5 in the column *raw distribution*. From these results, it can be concluded that this approach provides accurate NP sizing (errors below 5% for the NP diameter, corresponding to errors below 15% in the NP volume) for NPs with a nominal diameter above 100 nm, with particle number density and mass concentration recoveries ranging between 87.0 and 99.5%. For 80 and 100 nm, however, the results obtained with the raw distributions reflect the overlap with the background signal. This was especially noticeable in the low recoveries obtained for particle number densities (56.3 – 66.3 %), and the aberrant results for NP sizing. In fact, the NP diameter was shown to be significantly higher than the values obtained by TEM, which is certainly related to an incorrect average size calculation (biased high) due to the impossibility to discriminate the signals from the smaller NPs, also present in the NP distribution, from the background. The mass concentration derived from the raw distributions was found to be less affected by this problem, which needs to be attributed to a significant contribution of the background signal to the NP mass concentrations and to the fact that the detectable NPs are the larger/heavier ones, thus contributing to a higher extent to the final mass concentration.

In order to improve the characterization of SiO_2 NPs in those cases in which the distribution partially overlaps with the background, a straightforward and user-friendly approach was evaluated. This approach was based on a deconvolution of the overlapping distributions of background signals and NP signals using the OriginLab data analysis and graphing software. The deconvolution was used to resolve or decompose the overlapping peaks into their separate components (deconvolution was

also applied by Cornelis and Hassellöv in order to discriminate smaller NPs by SP-ICP-MS).[50] Thus, by applying a simple deconvolution, a corrected distribution for the corresponding NPs was generated by approximating the "raw" distribution by a Gaussian function (see Equation 2).

$$y = y_0 + \frac{A}{w\sqrt{\pi/2}} * e^{-2\frac{(x-x_0)^2}{w^2}} \qquad \text{Equation 2}$$

where y_0 = offset, x_0 = center, w = width and A = area.

Application of this deconvolution method becomes more successful as the intensity of the NP distribution peak (number of NPs detected) is maximized relative to the background distribution peak (number of events identified as background). Due to the specific conditions of this work – *i.e.* slight ionic analyte contamination – this could only be done by increasing the concentration of the NP suspension (as extending the measurement time would increase both peaks proportionally). Unfortunately, this comes at the cost of an increased probability for double events to occur. Thus, as can be seen from Table 1, suspensions for the NPs of 80 nm using the H_2 – on-mass approach, and 100 nm for the CH_3F – mass-shift approach were more concentrated (in terms of particles L^{-1}) for this reason. With the dilution factors used, an increased probability of double events up to 10% in the case of H_2 – on-mass, and 28% in the case of CH_3F – mass-shift was calculated; nevertheless, this option was preferred as it is the only way to obtain accurate results for the sizing of these NPs. An example of the use of this approach is presented in Figure 6, in which it can be seen that both background and NP distributions approximate their corresponding functions well. Therefore, the use of this approach should enable the characterization of SiO_2 NPs that cannot be fully resolved from the background signal.

In order to evaluate the suitability of the deconvolution approach for characterization of NP distributions, the method was applied to SiO_2 NPs with particle sizes higher than 100 nm *i.e.* fully resolved, as well as to SiO_2 NP distributions not fully resolved from the background, *i.e.* 80 and 100 nm (H_2) and 100 nm (CH_3F). The results obtained are shown in Table 5, under the designation *deconvolution approach*. It can be seen that accurate results for particle diameter, particle number

density and mass concentration were achieved when applying the corresponding model to complete NP distributions, which validates the use of the Gaussian fitting for the NP distributions. For the NP distributions partially overlapping the background, accurate sizes were obtained in all cases, while particle number densities deviated slightly from the expected values (81.6 – 105.8% recoveries). The latter observation can be explained by the design of the experiment itself. In fact, and as seen from Figure 6 for H_2 mode, the right part of the NP distribution is not fully coincident with the model, which could indicate the existence of a second population of double events, resulting from the relatively high particle number density used for this experiment. This second distribution does not seem to significantly affect sizing of the primary distribution, and accurate results are obtained for this parameter upon application of the deconvolution model. The particle number density values, on the other hand, cannot be 100% accurate if double events are occurring, although results for this parameter with the deconvolution model are much closer to the expected values than with the raw distributions.

As a final test for method robustness, calibration curves for the different NPs measured were drawn and are shown in Figure 7. It has been shown that linearity for these calibration plots can be lost due to different factors, two of which have been identified as the most serious.[51] On the one hand, the linear dynamic range of electron multipliers operated in pulse counting mode is limited, although this problem can be easily solved working in dual detection mode (pulse counting and analog modes), provided adequate cross-calibration at the beginning of the measuring session.[38] A more serious problem can arise due to different degrees of vaporization/ionization for the smaller and the larger particles, which may require specific optimization of the measuring conditions for SP-ICP-MS, especially concerning forward ICP power and sample gas flow rate.[38, 51] As seen from Figure 7, however, linear calibration curves (R^2 = 0.9997 and 0.9998 for H_2 – on mass and CH_3F – mass shift approaches, respectively) were obtained in this case covering the entire range of NP sizes studied (80 – 400 nm diameter), which is in good agreement with literature for SiO_2 NPs.[2, 38, 39, 52] It is interesting to point out that data shown in the calibration plots were obtained on different days and that no

specific optimization other than that reported in section 3.1 was performed for measurement of the NPs, which indicates that the methods developed are robust for characterizing SiO_2 NPs of different sizes in the range of 80 to 400 nm.

4. CONCLUSION

In this work, the capabilities of ICP-MS/MS using different operation modes *i.e.* no gas or "vented" mode, He "KED" mode, and H_2, O_2, NH_3 and CH_3F "chemical resolution" modes, were evaluated for obtaining interference-free conditions for ultra-trace Si determination. After a comprehensive study, the H_2 – on-mass and of CH_3F – mass-shift modes were selected to avoid spectral overlap, providing an instrumental LoD < 15 ng L^{-1}. The methods developed were evaluated for characterizing SiO_2 NPs (ranging between 80 and 400 nm) *via* SP-ICP-MS/MS. The use of a conventional approach was demonstrated to provide accurate particle size, particle number density and mass concentration for sizes > 100 nm, while for 80 and 100 nm, the distribution was found to be partially overlap with that of the background signals. Despite some dissolved Si contamination (BEC = 0.29 ± 0.02 µg L^{-1}), the use of a simple deconvolution approach following a Gaussian model enabled acceptable results to be obtained for NPs of 80 and 100 nm as well, which are the lowest SiO_2 NP sizes that have been detected so far *via* SP-ICP-MS with instrumentation only allowing for the use of dwell times in the ms range, *i.e.* without splitting the signal of a single NP in various events. Although SP-ICP-MS/MS has been scarcely used to date for NP characterization, it is expected that the results obtained in this work and the recent development of faster ICP- tandem mass spectrometers (with dwell times as low as 0.1 ms) will open new possibilities in this field in the near future.

ACKNOWLEDGEMENTS

The authors acknowledge the funding from CTQ2015-64684-P (MINECO/FEDER) and the Aragón Government (Fondo Europeo de Desarrollo Regional y FEDER Aragón 2014-2020). This work was supported by CNPq, Conselho Nacional de Desenvolvimiento Científico e Tecnológico – Brazil (232487/2014-6). FV acknowledges the Special Research Fund of Ghent University BOF-UGent for

financial support. The Ghent University authors acknowledge Agilent Technologies for providing them with an ACT-UR research project grant.

References

1. P. Krystek, A. Ulrich, C. C. Garcia, S. Manohar and R. Ritsema, *J. Anal. At. Spectrom.*, 2011, **26**, 1701 - 1721.
2. M. D. Montaño, B. J. Majestic, A. K. Jämting, P. Westerhoff and J. F. Ranville, *Anal. Chem.*, 2016, **88**, 4733 - 4711.
3. J. Heroult, V. Nischwitz, D. Bartczak and H. Goenaga-Infante, *Anal. Bioanal. Chem.*, 2014, **406**, 3919 - 3927.
4. D. Bartczak, P. Vincent and H. Goenaga-Infante, *Anal. Chem.*, 2015, **87**, 5482 - 5485.
5. D. Speed, P. Westerhoff, R. Sierra-Alvarez, R. Draper, P. Pantano, S. Aravamudhan, K. L. Chen, K. Hristovski, P. Herckes, X. Bi, Y. Yang, C. Zeng, L. Otero-Gonzalez, C. Mikoryak, B. A. Wilson, K. Kosaraju, M. Tarannum, S. Crawford, P. Yi, X. Liu, S. V. Babu, M. Moinpour, J. Ranville, M. Montano, C. Corredor, J. Posner and F. Shadman, *Environ. Sci.:Nano*, 2015, **2**, 227 - 244.
6. W. Lin, Y.-w. Huang, X.-D. Zhou and Y. Ma, *Toxicol. Appl. Pharmacol.*, 2006, **217**, 252 - 259.
7. R. D. Handy, R. Owen and E. Valsami-Jones, *Ecotoxicology*, 2008, **17**, 315 - 325.
8. M. Hassellöv, J. W. Readman, J. F. Ranville and K. Tiede, *Ecotoxicology*, 2008, **17**, 344 - 361.
9. Commission Recommendation 2011/696/EU, OJ L 275, 20.10.2011.
10. J. Tuoriniemi, A. J. H. Johnsson, J. P. Holmberg, S. Gustafsson, J. A. Gallego-Urrea, E. Olson, J. B. C. Petterson and M. Hassellöv, *Sci. Technol. Adv. Mater.*, 2014, **15**, 1 - 10.
11. A. K. Brewer and A. M. Striegel, *Anal. Chem.*, 2011, **83**, 3068 - 3075.
12. H. E. Pace, N. J. Rogers, C. Jarolimek, V. A. Coleman, E. P. Gray, C. P. Higgins and J. F. Ranville, *Environ. Sci. Technol.*, 2012, **46**, 12272 - 12280.
13. M. Resano, E. Garcia-Ruiz and R. Garde, *J. Anal. At. Spectrom.*, 2016, **31**, 2233 - 2241.
14. F. Laborda, E. Bolea and J. Jiménez-Lamana, *Anal. Chem.*, 2014, **86**, 2270 - 2278.
15. S. Lee, X. Bi, R. B. Reed, J. F. Ranville, P. Herckes and P. Westerhoff, *Environ. Sci. Technol.*, 2014, **48**, 10291 - 10300.

16. F. Laborda, J. J. Jiménez-Lamana, E. Bolea and J. R. Castillo, *J. Anal. At. Spectrom.*, 2011, **26**, 1362 - 1371.

17. B. Meermann and F. Laborda, *J. Anal. At. Spectrom.*, 2015, **30**, 1226 - 1228.

18. J. Tuorinieni, G. Cornelis and M. Hasselöv, *J. Anal. At. Spectrom.*, 2015, **30**, 1723 - 1729.

19. L. Telgmann, C. D. Metcalfe and H. Hintelmann, *J. Anal. At. Spectrom.*, 2014, **29**, 1265 - 1272.

20. J. Liu, K. E. Murphy, R. I. MacCuspie and M. R. Winchester, *Anal. Chem.*, 2014, **86**, 3405 - 3414.

21. M. D. Montaño, J. W. Olesik, A. G. Berber, K. Challis and J. R. Ranville, *Anal. Bioanal. Chem.*, 2016, **408**, 5053 - 5074.

22. N. Jakubowski, L. Moens and F. Vanhaecke, *Spectrochim. Acta, Part B*, 1998, **53**, 1739 - 1763.

23. L. Moens and N. Jakubowski, *Anal. Chem.*, 1998, **70**, 251A - 256A.

24. N. Jakubowski, T. Prohaska, L. Rottmann and F. Vanhaecke, *J. Anal. At. Spectrom.*, 2011, **26**, 693 - 726.

25. I. Strenge and C. Engelhard, *J. Anal. At. Spectrom.*, 2016, **31**, 135 - 144.

26. S. Diez Fernández, N. Sugishama, J. Ruiz Encinar and A. Sanz-Medel, *Anal. Chem.*, 2012, **84**, 5851 - 5857.

27. L. Balcaen, G. Woods, M. Resano and F. Vanhaecke, *J. Anal. At. Spectrom.*, 2013, **28**, 33 - 39.

28. L. Balcaen, E. Bolea-Fernandez, M. Resano and F. Vanhaecke, *Anal. Chim. Acta*, 2015, **894**, 7 - 19.

29. E. Bolea-Fernandez, L. Balcaen, M. Resano and F. Vanhaecke, *J. Anal. At. Spectrom.*, 2017, DOI: 10.1039/C7JA00010C.

30. L. Balcaen, E. Bolea-Fernandez, M. Resano and F. Vanhaecke, *Anal. Chim. Acta*, 2014, **809**, 1 - 8.

31. E. Bolea-Fernandez, L. Balcaen, M. Resano and F. Vanhaecke, *Anal. Chem.*, 2014, **86**, 7969 - 7977.

32. E. Bolea-Fernandez, L. Balcaen, M. Resano and F. Vanhaecke, *J. Anal. At. Spectrom.*, 2016, **31**, 303 - 310.

33. R. S. Amais, C. D. B. Amaral, L. L. Fialho, D. Schiavo and J. A. Nóbrega, *Anal. Methods*, 2014, **6**, 4516 - 4520.

34. A. Virgilio, R. S. Amais, C. D. B. Amaral, L. L. Fialho, D. Schiavo and J. A. Nóbrega, *Spectrochim. Acta, Part B*, 2016, **126**, 31 - 36.

35. M. Menendez-Miranda, M. T. Fernandez-Arguelles, J. M. Costa-Fernandez, J. Ruiz Encinar and A. Sanz-Medel, *Anal. Chim. Acta*, 2014, **839**, 8 - 13.

36. M. Menendez-Miranda, J. Ruiz Encinar, J. M. Costa-Fernandez and A. Sanz-Medel, *J. Chromatogr. A*, 2015, **1422**, 247 - 252.

37. F. Aureli, M. D'Amato, A. Raggi and F. Cubadda, *J. Anal. At. Spectrom.*, 2015, **30**, 1266 1273.

38. J. W. Olesik and P. J. Gray, *J. Anal. At. Spectrom.*, 2012, **27**, 1143 - 1155.

39. R. Peters, Z. Herrera-Rivera, A. Unndas, M. van der Lee, H. Marvin, H. Bouwmeester and S. Weigel, *J. Anal. At. Spectrom.*, 2015, **30**, 1274 - 1285.

40. H. E. Pace, N. J. Rogers, C. Jarolimek, V. A. Coleman, C. P. Higgins and J. F. Ranville, *Anal. Chem.*, 2011, **83**, 9361 - 9369.

41. I. Feldmann, N. Jakubowski and D. Stuewer, *Fresenius J. Anal. Chem.*, 1999, **365**, 415 - 421.

42. S. D. Tanner, V. I. Baranov and U. Vollkopf, *J. Anal. At. Spectrom.*, 2000, **15**, 1261 - 1269.

43. M. Resano, M. Aramendía, A. B. Volynsky and M. A. Belarra, *Spectrochim. Acta Part B*, 2004, **59**, 523 - 531.

44. I. De Schrijver, M. Aramendía, M. Resano, A. Dumoulin and F. Vanhaecke, *J. Anal. At. Spectrom.*, 2008, **23**, 500 - 507.

45. S. D. Tanner, V. I. Baranov and D. R. Bandura, *Spectrochim. Acta Part B*, 2002, **57**, 1361 - 1452.

46. A. Gourgiotis, T. Ducasse, E. Barker, P. Jollivet, S. Gin, S. Bassot and C. Cazala, *Anal. Chim. Acta*, 2017, **954**, 68 - 76.

47. S. Gschwind, L. Flamigni, J. Koch, O. Borovinskaya, S. Groh, K. Niemax and D. Günther, *J. Anal. At. Spectrom.*, 2011, **26**, 1166 - 1174.

48. I. Abad-Álvaro, E. Peña-Vázquez, E. Bolea, P. Bermejo-Barrera, J. R. Castillo and F. Laborda, *Anal. Bioanal. Chem.*, 2016, **408**, 5089 - 5097.

49. M. Yamanaka and T. Itagaki, *Agilent Technical note*, 2016, 5991-6596EN, http://www.agilent.com/cs/library/applications/5991-6596EN.pdf.

50. G. Cornelis and M. Hassellöv, *J. Anal. At. Spectrom.*, 2014, **29**, 134 - 144.

51. W.-W. Lee and W.-T. Chan, *J. Anal. At. Spectrom.*, 2015, **30**, 1245 - 1254.

52. C. C. Garcia, A. Murtazin, S. Groh, V. Horvatic and K. Niemax, *J. Anal. At. Spectrom.*, 2010, **25**, 645 - 653.

Figure 1. Full mass spectra in the range of interest (2 – 100 amu) obtained by product ion scanning for 10 µg L^{-1} Si standard solution with the addition of H_2 (5 mL min^{-1} - A), O_2 (0.2 mL min^{-1} - B), NH_3 (1 mL min^{-1} – C) or CH_3F (0.5 mL min^{-1} – D) reaction gas. The best-suited reaction product ions finally selected are indicated in bold.

Figure 2. Selection of the optimum gas flow rate for the product ions selected in the case of (A) H_2 – (Si^+ and SiH^+, 1.5 and 4.5 mL min^{-1}, respectively), (B) O_2 (SiO^+, 0.25 mL min^{-1}), (C) NH_3 ($SiNH_2^+$, 1.0 mL min^{-1}) and (D) CH_3F (SiF^+, 0.5 mL min^{-1}).

Figure 3. Frequency distribution for the lowest NP sizes detectable using the different approaches evaluated in this work. Practical $LODs_{size}$ are indicated in red in each figure. Frequency refers to the number of events of each type (background or NP) detected.

Figure 4. Frequency distributions of SiO_2 NP suspensions (0.1 – 5 µg L^{-1}) with different NP diameters (ranging between 80 and 400 nm) when using H_2 in an on-mass approach. Frequency refers to the number of events of each type (background signal or NP) detected.

Figure 5. Particle size distributions calculated for SiO_2 NP suspensions of different sizes ranging from 80 to 400 nm using H_2 (on-mass) and CH_3F (mass-shift) approaches in ICP-MS/MS, with concentrations of the SiO_2 NP suspensions ranging between 0.1 – 5 and 0.5 – 5 µg L^{-1} for H_2 and CH_3F, respectively. Normalized frequency refers to the number of NPs detected of each size normalized to the number of NPs counted at the peak maximum.

Figure 6. Deconvolution of the signal distribution of 80 nm SiO_2 NPs, overlapping with the background signal distribution for SP-ICP-MS/MS using a H_2 – on-mass approach and following a Gaussian model.

Figure 7. Calibration curves for the SiO_2 NPs with diameters of 80 (only H_2 – on mass), 100, 200, 300 and 400 nm obtained with the H_2 – on mass and CH_3F – mass shift methods.

Table 1. Information on particle size (TEM), particle number density and mass concentration (gravimetric analysis), and dilution factors used for the measurement of the SiO_2 NP dispersions used in this work. Values for the stock solutions are those provided by nanoComposix.

Nominal NP size (nm)	NP reference size (mean) (nm)	Particle number density stock solution (particles mL^{-1})	Mass concentration SiO_2 stock solution (g L^{-1})	Dilution factor H_2 (on-mass) mode	Dilution factor CH_3F (mass-shift) mode
80	82.6 ± 4.7	1.5×10^{13}	10.0	1×10^{8}	--
100	99.2 ± 5.8	9.5×10^{12}	10.7	1×10^{8}	2×10^{7}
200	197 ± 14	1.1×10^{12}	10.1	1×10^{7}	1×10^{7}
300	297 ± 12	3.4×10^{11}	10.4	1×10^{7}	4×10^{6}
400	401 ± 26	1.4×10^{11}	10.3	2×10^{6}	2×10^{6}

Table 2. Instrument settings for the Agilent 8800 (ICP-MS/MS).

	No gas "Vented" mode		He	H_2 On mass		H_2 Mass-shift	O_2	NH_3	CH_3F
Scan type	SQ	MS/MS	MS/MS	SQ	MS/MS	MS/MS	MS/MS	MS/MS	MS/MS
Plasma mode	Low matrix		Low matrix	Low matrix		Low matrix	Low matrix	Low matrix	Low matrix
Rf power (W)	1550		1550	1550		1550	1550	1550	1550
Carrier gas flow rate (L min^{-1})	1.11		1.11	1.11		1.11	1.11	1.12	1.11
Extract 1 (V)	0.0		0.0	0.0		0.0	0.0	-3.0	-3.0
Q1 bias(V)	-3.0	0.0	0.0	-2.0	0.0	0.0	0.0	-1.0	-1.0
Octopole bias (V)	-8.0		-18.0	-18.0		-21.0	-5.0	-5.0	-5.0
Energy discrimination (V)	5.0		5.0	0.0		-5.0	-8.0	-8.4	-10.0
He flow (mL min^{-1})	---		1.5	---		---	---	1.0	---
H_2 flow (mL min^{-1})	---		---	1.5		4.5	---	---	---
3^{rd} gas flow (mL min^{-1})	---		---	---		---	---	1.0	---
4^{th} gas flow (mL min^{-1})	---		---	---		---	0.25	---	0.5
Q1 → Q2 masses	28 → 28		28 → 28	28 → 28		28 → 29	28 → 44	28 → 44	28 → 47
Extract 2 (V)	-180.0		-180.0	-170.0		-130.0	-145.0	-190.0	-190.0
Q2 bias (V)	-3.0		-13.0	-18.0		-26.0	-13.0	-13.4	-15.0
Wait time offset (ms)	0		0	0		0	0	0	0
Integration time (TRA) (ms)	3		3	3		3	3	3	3
Total analysis time/sample (s)	60		60	60		60	60	60	60

Table 3. Summary of the reaction pathways of Si^+ and interfering ions for different operation modes

(1) No gas – "Vented mode"	**(2) Helium – He "KED mode"**
$^{28}Si^+ \rightarrow {}^{28}Si^+$ (on-mass)	$^{28}Si^+ + He \rightarrow {}^{28}Si^+$ (on-mass)
$^{28}CO^+ \rightarrow {}^{28}CO^+$	$^{28}CO^+ + He \rightarrow$ Removed by collisions + KED
$^{28}N_2^+ \rightarrow {}^{28}N_2^+$	$^{28}N_2^+ + He \rightarrow$ Removed by collisions + KED
(3) Hydrogen – H_2	**(4) Oxygen – O_2**
$^{28}Si^+ + H_2 \rightarrow {}^{28}Si^+$ (on-mass)	$^{28}Si^+ + O_2 \rightarrow {}^{44}SiO^+$ (mass-shift)
$^{28}Si^+ + H_2 \rightarrow {}^{29}SiH^+$ (mass-shift)	$^{28}Si^+ + O_2 \rightarrow {}^{60}SiO_2^+$ (mass-shift)
$^{28}CO^+ + H_2 \rightarrow {}^{29}COH^+ + H^+$	$^{28}CO^+ + O_2 \rightarrow {}^{44}CO_2^+$
$^{28}N_2^+ + H_2 \rightarrow {}^{29}N_2H^+ + H^+$	$^{28}N_2^+ + O_2 \rightarrow {}^{44}N_2O^+$
(5) Ammonia – NH_3	**(6) Methyl fluoride – CH_3F**
$^{28}Si^+ + NH_3 \rightarrow {}^{44}SiNH_2^+$ (mass-shift)	$^{28}Si^+ + CH_3F \rightarrow {}^{44}SiF^+ + CH_3$ (mass-shift)
$^{28}CO^+ + NH_3 \rightarrow$ No reaction	$^{28}CO^+ + CH_3F \rightarrow$ No reaction
$^{28}N_2^+ + NH_3 \rightarrow$ No reaction	$^{28}N_2^+ + CH_3F \rightarrow$ No reaction

Table 4. Calibration data and instrumental limits of detection (LoDs) and of quantification (LoQs) obtained for Si determination using ICP-MS/MS operated in different modes. LoDs and LoQs were calculated as 3 and 10 times the standard deviation on 10 consecutive measurements of a blank solution (MQ H_20), divided by the slope of the calibration curve, respectively.

Gas	Mode	Approach	Q1 (amu)	Q2 (amu)	Sensitivity (L counts s^{-1} μg^{-1})	Intercept (counts s^{-1})	R^2	LoD ($\mu g\ L^{-1}$)	LoQ ($\mu g\ L^{-1}$)
No gas	SQ	On-mass	--	28	34800	830000	0.9996	0.9	3
	MS/MS	On-mass	28	28	21800	76100	0.9996	0.05	0.2
He	MS/MS	On-mass	28	28	287	471	0.9992	0.2	0.6
H_2	SQ	On-mass	--	28	43700	24300	0.9991	0.05	0.2
	MS/MS	On-mass	28	28	26900	7430	0.99998	0.02	0.05
	MS/MS	Mass-shift	28	29	4980	4240	0.9998	0.05	0.2
O_2	MS/MS	Mass-shift	28	44	8700	2470	0.9998	0.02	0.05
NH_3	MS/MS	Mass-shift	28	44	3160	948	0.99998	0.03	0.1
CH_3F	MS/MS	Mass-shift	28	47	13100	4070	0.9997	0.01	0.03

Table 5. Characterization of SiO_2 NPs using CH_3F (mass-shift) and H_2 (on-mass) as reaction gases in ICP-MS/MS

Methyl fluoride (CH_3F) – MS/MS – Mass-shift approach						
Particle diameter (TEM) (nm)[a]	**Particle diameter (nm)[b]**		**Particle number density Recovery (%)[c]**		**Mass concentration Recovery (%)[c]**	
	Raw distribution	**Deconvolution approach**	**Raw distribution**	**Deconvolution approach**	**Raw distribution**	**Deconvolution approach**
99.2 ± 5.8	106 ± 20	94 ± 13	57 ± 2	82 ± 2	90 ± 3	94 ± 4
197.1 ± 13.5	191 ± 19	188 ± 16	94 ± 8	100 ± 8	100 ± 4	105 ± 3
297.2 ± 11.5	282 ± 24	283 ± 14	94 ± 1	100 ± 1	95 ± 1	101 ± 2
401.0 ± 25.5	378 ± 34	368 ± 12	92 ± 2	105 ± 2	95 ± 2	101 ± 2
Hydrogen (H_2) – MS/MS – On-mass approach						
Particle diameter (TEM) (nm)[a]	**Particle diameter (nm)[b]**		**Particle number density Recovery (%)[c]**		**Mass concentration Recovery (%)[c]**	
	Raw distribution	**Deconvolution approach**	**Raw distribution**	**Deconvolution approach**	**Raw distribution**	**Deconvolution approach**
82.6 ± 4.7	90 ± 9	80 ± 10	64 ± 3	106 ± 4	100 ± 3	111 ± 2
99.2 ± 5.8	104 ± 15	93 ± 12	66 ± 2	84 ± 6	98 ± 2	94 ± 6
197.1 ± 13.5	191 ± 18	190 ± 14	87 ± 3	101 ± 2	92 ± 3	107 ± 2
297.2 ± 11.5	285 ± 15	286 ± 12	93 ± 2	97 ± 5	96 ± 2	102 ± 7
401.0 ± 25.5	381 ± 37	373 ± 16	90 ± 2	95 ± 4	96 ± 3	108 ± 8

[a] Uncertainty values for the particle diameter determined by TEM are those provided by the manufacturer and correspond to the standard deviation of the size distribution for the NPs.
[b] Uncertainty values for the particle diameter determined by SP-ICP-MS/MS correspond to the standard deviation of the size distribution for the NPs.
[c] Uncertainty values for the particle number density and mass concentration recoveries correspond to the standard deviation of three replicate measurements of 60 s each.

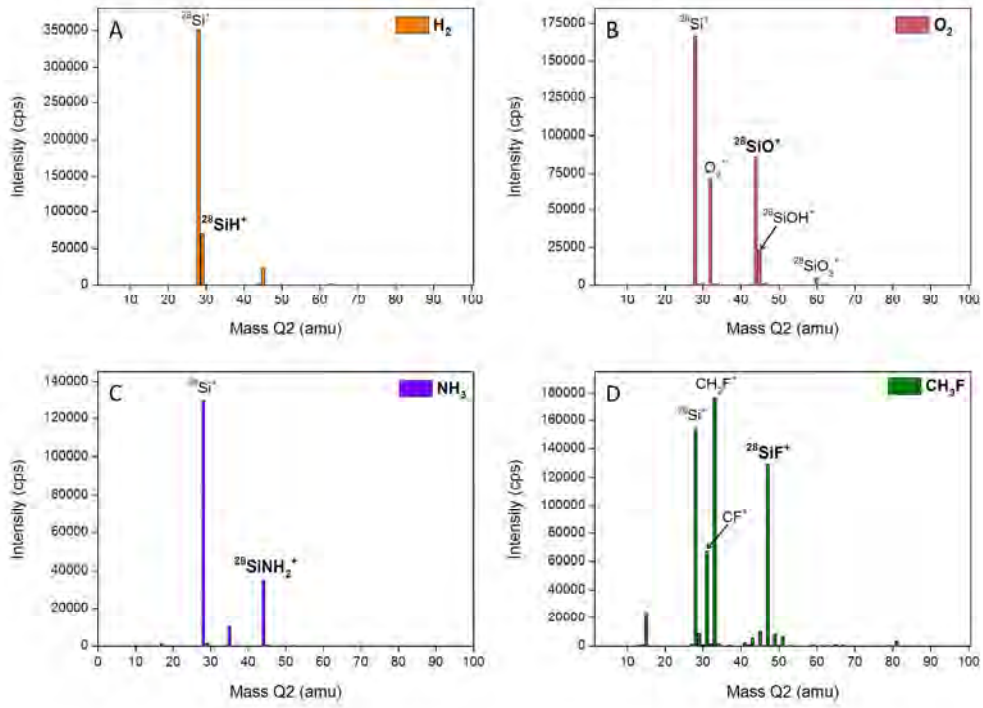

Figure 1. Full mass spectra in the range of interest (2 – 100 amu) obtained by product ion scanning for 10 µg L^{-1} Si standard solution with the addition of H_2 (5 mL min^{-1} - A), O_2 (0.2 mL min^{-1} - B), NH3 (1 mL min-1 – C) or CH_3F (0.5 mL min^{-1} – D) reaction gas. The best-suited reaction product ions finally selected are indicated in bold.

254x190mm (300 x 300 DPI)

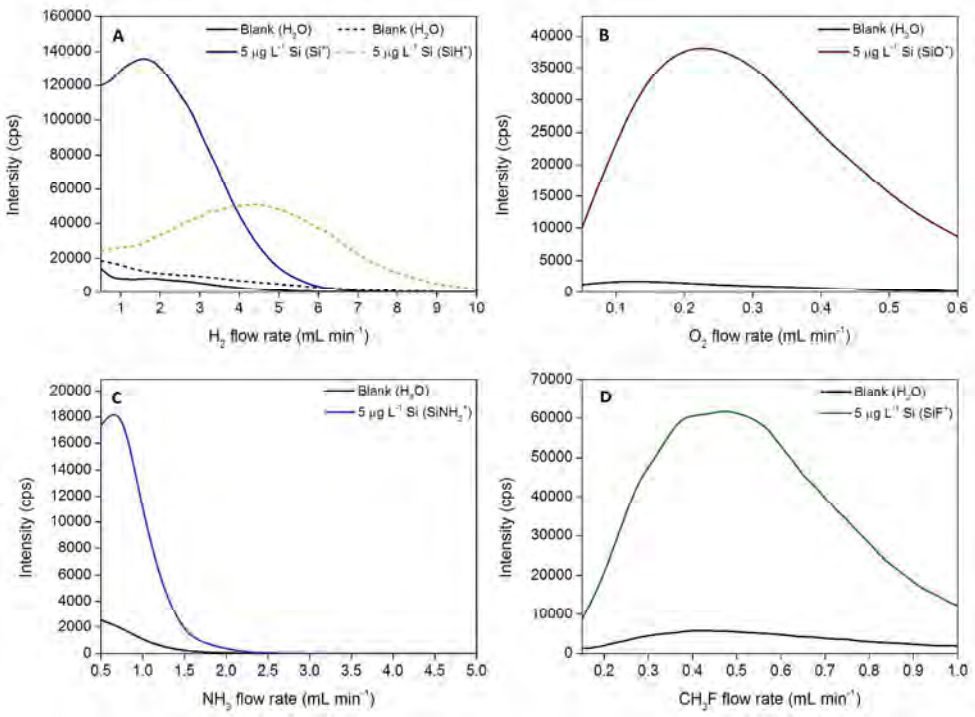

Figure 2. Selection of the optimum gas flow rate for the product ions selected in the case of (A) H_2 –(Si^+ and SiH^+, 1.5 and 4.5 mL min^{-1}, respectively), (B) O_2 (SiO^+, 0.25 mL min^{-1}), (C) NH_3 ($SiNH_2^+$, 1.0 mL min^{-1}) and (D) CH_3F (SiF^+, 0.5 mL min^{-1}).

254x190mm (300 x 300 DPI)

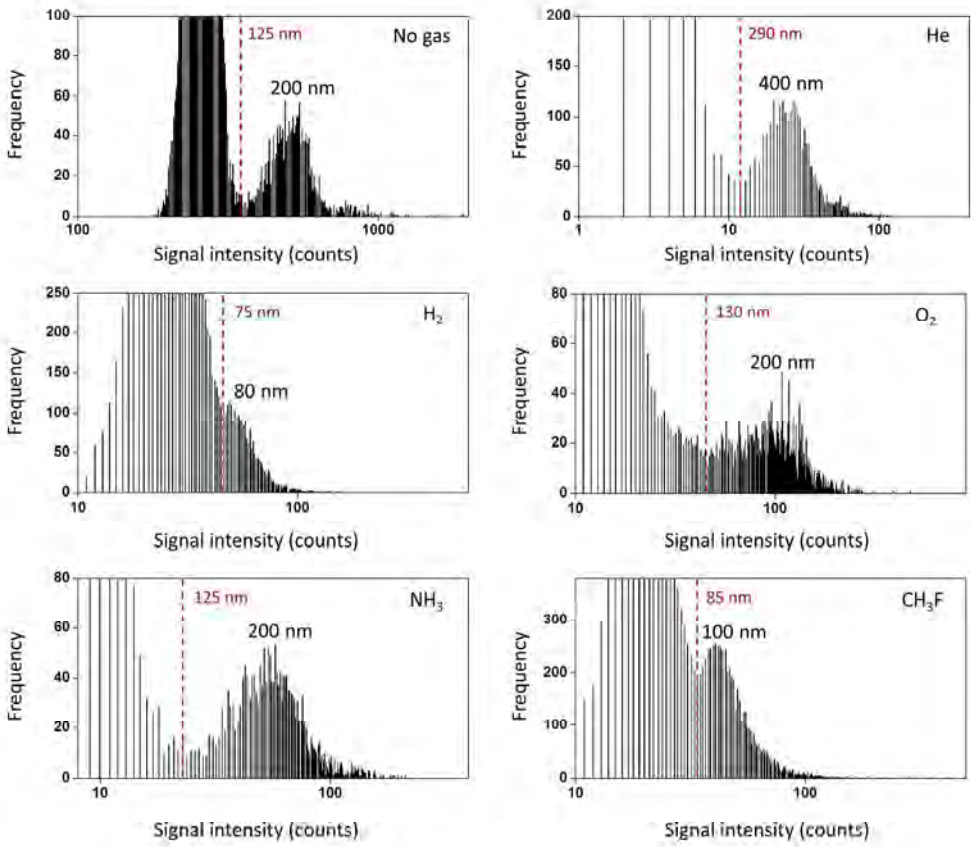

Figure 3. Frequency distribution for the lowest NP sizes detectable using the different approaches evaluated in this work. Practical $LODs_{size}$ are indicated in red in each figure. Frequency refers to the number of events of each type (background or NP) detected.

199x199mm (300 x 300 DPI)

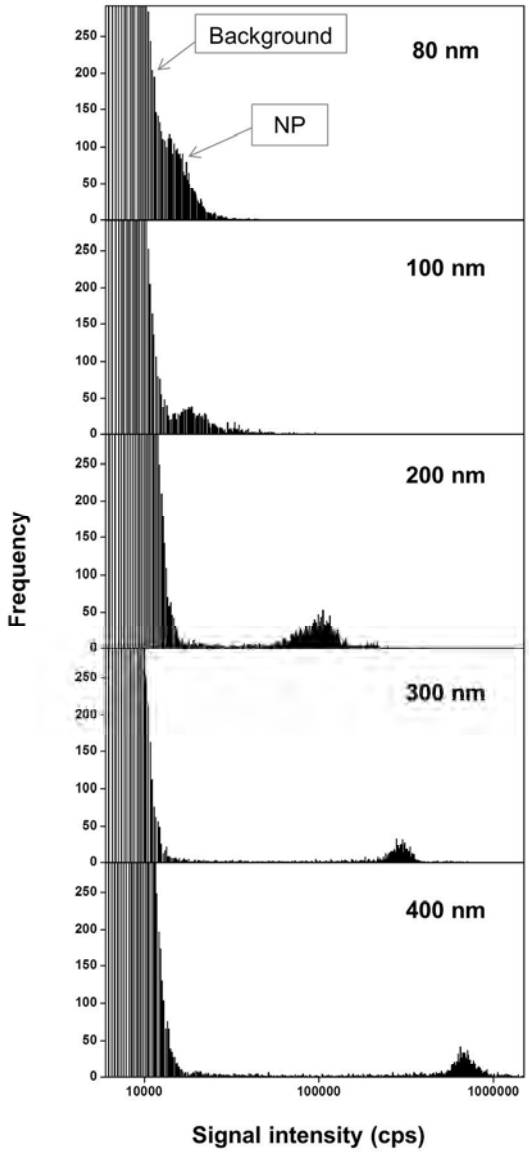

Figure 4. Frequency distributions of SiO_2 NP suspensions (0.1 – 5 µg L^{-1}) with different NP diameters (ranging between 80 and 400 nm) when using H_2 in an on-mass approach. Frequency refers to the number of events of each type (background signal or NP) detected.

190x254mm (300 x 300 DPI)

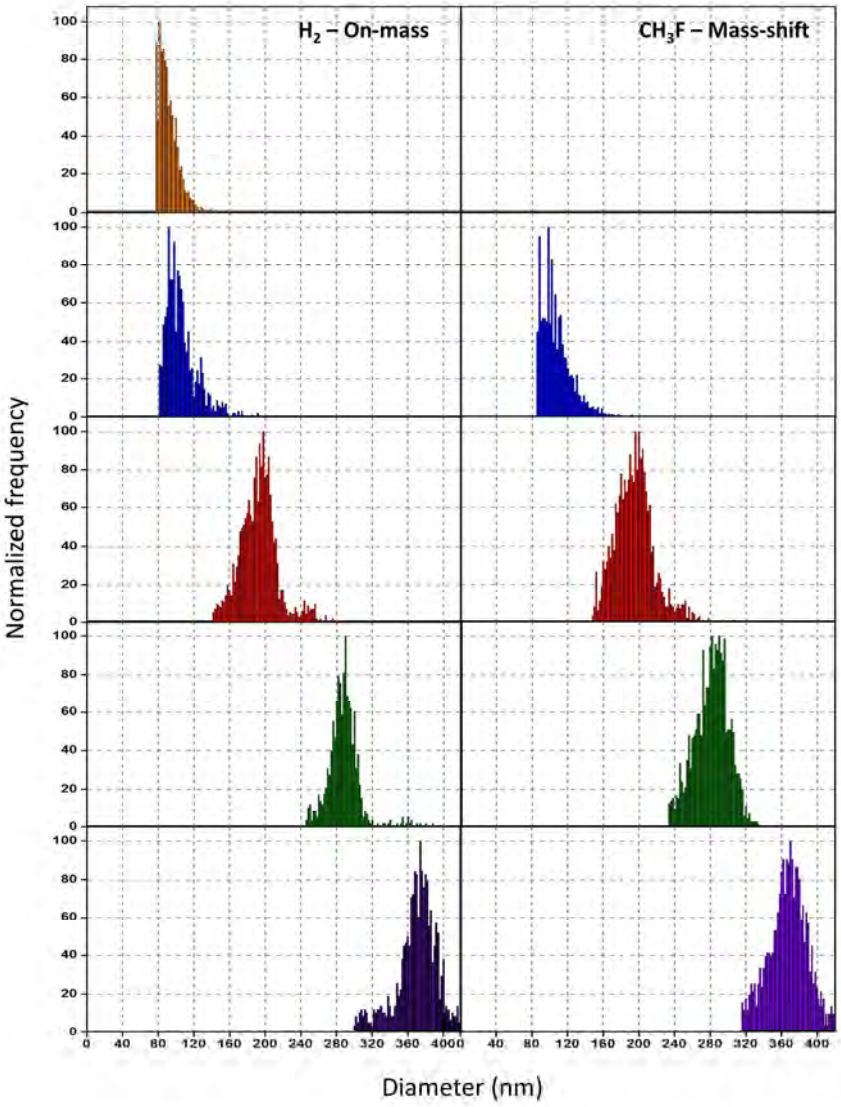

Figure 5. Particle size distributions calculated for SiO_2 NP suspensions of different sizes ranging from 80 to 400 nm using H_2 (on-mass) and CH_3F (mass-shift) approaches in ICP-MS/MS, with concentrations of the SiO_2 NP suspensions ranging between 0.1 – 5 and 0.5 – 5 µg L^{-1} for H_2 and CH_3F, respectively. Normalized frequency refers to the number of NPs detected of each size normalized to the number of NPs counted at the peak maximum.

190x250mm (300 x 300 DPI)

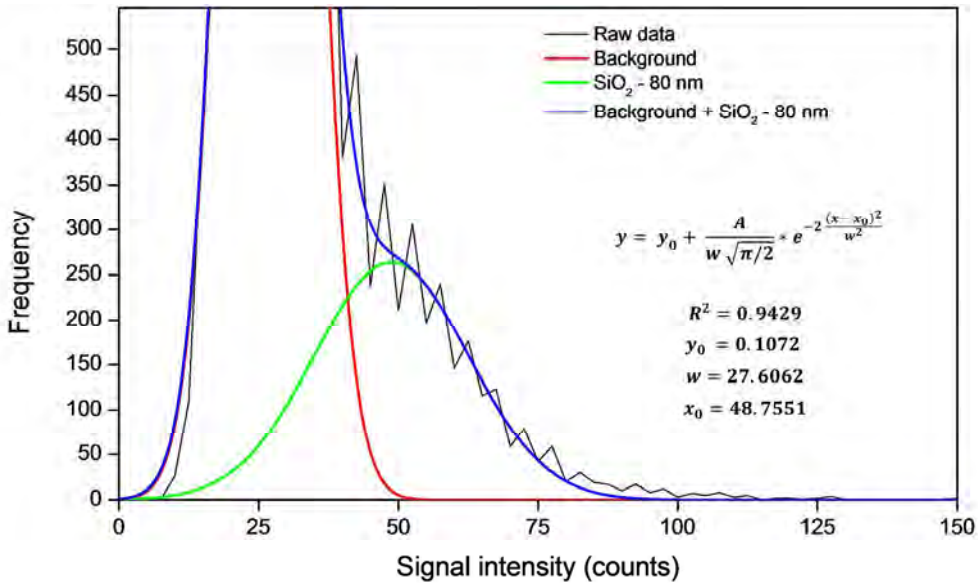

Figure 6. Deconvolution of the signal distribution of 80 nm SiO_2 NPs, overlapping with the background signal distribution for SP-ICP-MS/MS using a H_2 – on-mass approach and following a Gaussian model.

254x190mm (300 x 300 DPI)

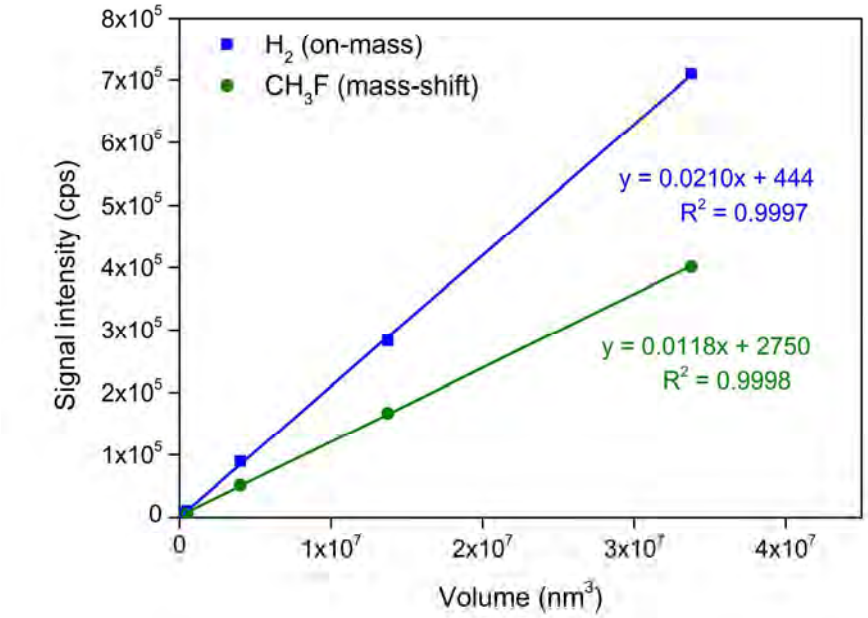

Figure 7. Calibration curves for the SiO_2 NPs with diameters of 80 (only H_2 – on mass), 100, 200, 300 and 400 nm obtained with the H_2 – on mass and CH_3F – mass shift methods.

199x139mm (300 x 300 DPI)